



## **Efficacy of targeting bone-specific GIP receptor in ovariectomy-induced bone loss**

Guillaume Mabillean, Benoit Gobron, Aleksandra Mieczkowska, Rodolphe Perrot, Daniel Chappard

### **► To cite this version:**

Guillaume Mabillean, Benoit Gobron, Aleksandra Mieczkowska, Rodolphe Perrot, Daniel Chappard. Efficacy of targeting bone-specific GIP receptor in ovariectomy-induced bone loss. *Journal of endocrinology*, 2018, 239 (2), pp.215-227. 10.1530/JOE-18-0214 . hal-02869273

**HAL Id: hal-02869273**

**<https://univ-angers.hal.science/hal-02869273>**

Submitted on 15 Jun 2020

**HAL** is a multi-disciplinary open access archive for the deposit and dissemination of scientific research documents, whether they are published or not. The documents may come from teaching and research institutions in France or abroad, or from public or private research centers.

L'archive ouverte pluridisciplinaire **HAL**, est destinée au dépôt et à la diffusion de documents scientifiques de niveau recherche, publiés ou non, émanant des établissements d'enseignement et de recherche français ou étrangers, des laboratoires publics ou privés.

1

2

EFFICACY OF TARGETING BONE-SPECIFIC GIP RECEPTOR IN OVARECTOMY-  
INDUCED BONE LOSS

3 Guillaume Mabileau<sup>1,2</sup>, Benoit Gobron<sup>1,3</sup>, Aleksandra Mieczkowska<sup>1</sup>, Rodolphe Perrot<sup>4</sup>,  
4 Daniel Chappard<sup>1,2,4</sup>

5 <sup>1</sup> Groupe d'Etudes Remodelage Osseux et bioMatériaux, GEROM, SFR 42-08, Université  
6 d'Angers, IRIS-IBS Institut de Biologie en Santé, CHU d'Angers, 49933 Angers cedex -  
7 France.



8 <sup>2</sup> Bone pathology unit, Angers university hospital, 49933 Angers cedex –France

9 <sup>3</sup> Rheumatology department, Angers university hospital, 49933 Angers cedex-France

10 <sup>4</sup> Service Commun d'Imageries et d'analyses microscopiques, SCIAM, SFR 42-08, Université  
11 d'Angers, IRIS-IBS Institut de Biologie en Santé, CHU d'Angers, 49933 ANGERS Cedex -  
12 FRANCE

13 ***Please send all correspondence to:***

Guillaume Mabileau, PhD  
GEROM-LHEA UPRES EA 4658  
Institut de Biologie en Santé  
Université d'Angers  
4 rue larrey  
49933 Angers Cedex 09  
France

 : +33(0) 244 688 450  
Fax : +33(0) 244 688 451  
 : [guillaume.mabileau@univ-angers.fr](mailto:guillaume.mabileau@univ-angers.fr)

14  
15 **Running title:** GIP in OVX-induced bone loss

16 **Abstract word count:** 230 words

17 **Manuscript word count:** 4,689 words

18 **Keywords:** GIP-Tag, GIP<sub>1-30</sub>, bone loss, bone matrix composition, bone microarchitecture  
19

## 20 **LIST OF ABBREVIATIONS**

- 21 5-FAM: 5 carboxy-fluorescein
- 22  $\alpha$ MEM: alpha minimum essential medium
- 23 AMPK $\alpha$ 2: AMP activated protein kinase alpha 2
- 24 ANCOVA: Analysis of covariance
- 25 ANOVA: Analysis of variance
- 26 BM: Bone marrow
- 27 BSA: Bovine serum albumin
- 28 cAMP: cyclic adenosine monophosphate
- 29 CREB: cAMP response element-binding protein
- 30 Ct.Ar: cortical area
- 31 Ct.Th: Cortical thickness
- 32 CtB: Cortical bone
- 33 CTx-I:
- 34 DPP-4: Dipeptidylpeptidase-4
- 35  $E_{IT}$ : Indentation modulus
- 36 FBS: Fetal bovine serum
- 37 FTIRM: Fourier transform infrared microspectroscopy
- 38 GIP: Glucose-dependent insulintropic polypeptide
- 39 GIPr: Glucose-dependent insulintropic polypeptide receptor
- 40  $H_{IT}$ : Indentation hardness
- 41  $I_{ap}$ : Moment of inertia about the anteroposterior axis
- 42  $I_{ml}$ : Moment of inertia about the mediolateral axis
- 43  $J$ : Polar moment of inertia
- 44 Ma.Ar: Marrow area
- 45 M-CSF: Macrophage-colony stimulating factor
- 46 MicroCT: X-ray microcomputed tomography
- 47 OVX: Ovariectomy

- 48 P1NP: N-terminal propeptide of type I procollagen
- 49 pHEMA: Poly(2-hydroxyethylmethacrylate)
- 50 pMMA: Poly(methylmethacrylate)
- 51 qBEI: Quantitative backscattered electron imaging
- 52 RANKL: Receptor activator of nuclear factor- $\kappa$ B ligand
- 53 STAT2: Signal transducer and activator of transcription 2
- 54 Tt.Ar: Total cross-sectional area
- 55  $W_{\text{plast}}$ : Dissipated energy

**56 ABSTRACT**

57 Glucose-dependent insulintropic polypeptide (GIP) has been recognized in the last decade  
58 as an important contributor of bone remodeling and is necessary for optimal bone quality.  
59 However, GIP receptors are expressed in several tissues in the body and little is known  
60 about the direct versus indirect effects of GIP on bone remodeling and quality. The aims of  
61 the present study were to validate two new GIP analogues, called [D-Ala<sup>2</sup>]-GIP-Tag and [D-  
62 Ala<sup>2</sup>]-GIP<sub>1-30</sub>, that specifically target either bone or whole body GIP receptors, respectively;  
63 and to ascertain the beneficial effects of GIP therapy on bone in a mouse model of  
64 ovariectomy-induced bone loss. Both GIP analogues exhibited similar binding capacities at  
65 the GIP receptor and intracellular responses as full-length GIP<sub>1-42</sub>. Furthermore, only [D-  
66 Ala<sup>2</sup>]-GIP-Tag, but not [D-Ala<sup>2</sup>]-GIP<sub>1-30</sub>, was undoubtedly found exclusively in the bone matrix  
67 and released at acidic pH. In ovariectomized animals, [D-Ala<sup>2</sup>]-GIP<sub>1-30</sub> but not [D-Ala<sup>2</sup>]-GIP-  
68 Tag ameliorated bone stiffness at the same magnitude than alendronate treatment. Only [D-  
69 Ala<sup>2</sup>]-GIP<sub>1-30</sub> treatment led to significant ameliorations in cortical microarchitecture. Although  
70 alendronate treatment increased the hardness of the bone matrix and the type B carbonate  
71 substitution in the hydroxyapatite crystals, none of the GIP analogues modified bone matrix  
72 composition. Interestingly, in ovariectomy-induced bone loss, [D-Ala<sup>2</sup>]-GIP-Tag failed to alter  
73 bone strength, microarchitecture and bone matrix composition. Overall, this study shows  
74 that the use of a GIP analogue that target whole body GIP receptors might be useful to  
75 improve bone strength in ovariectomized animals.

## 76 1. INTRODUCTION

77       Some evidences have emerged recently that the gut, and more specifically entero-  
78 endocrine cells, may play a role in maintaining optimal bone quality and bone mass (Gaudin-  
79 Audrain, et al. 2013; Henriksen, et al. 2003; Mabileau, et al. 2013; Mieczkowska, et al. 2013;  
80 Mieczkowska, et al. 2015b; Nissen, et al. 2014; Torekov, et al. 2014; Tsukiyama, et al. 2006;  
81 Walsh and Henriksen 2010; Xie, et al. 2005). Among the plethora of peptides secreted by the  
82 gastrointestinal tract, the glucose-dependent insulintropic polypeptide (GIP), synthesized  
83 and secreted by entero-endocrine K cells, has emerged as a potential candidate. Indeed,  
84 whole body GIP receptor (GIPr)-deficiency led to alterations of trabecular and cortical bone  
85 microarchitectures, tissue mineral density and collagen maturity (Gaudin-Audrain et al. 2013;  
86 Mieczkowska et al. 2013). Furthermore, administration of stable GIP analogues improved  
87 bone matrix composition and biomechanics at the tissue level in healthy and diabetic rodent  
88 models (Mabileau, et al. 2014; Mansur, et al. 2015; Mansur, et al. 2016).

89       In rodents, the GIPr is widely expressed in the body and expression has been  
90 documented in the endocrine pancreas, gastro-intestinal tract, adipose tissue, adrenal  
91 cortex, pituitary gland, vascular endothelium and several regions in the central nervous  
92 system (Baggio and Drucker 2007). Expression in bone has also been reported and the GIPr  
93 seems to be expressed in rodent and human osteoblasts, osteocytes and osteoclasts  
94 (Bollag, et al. 2000; Mabileau, et al. 2016; Mieczkowska, et al. 2015a). However, due to this  
95 wide variety of tissue expression, it is not clear whether the marked bone effects observed in  
96 previous rodent studies arise from inactivation/activation of bone-specific GIPr or  
97 extraskeletal GIPr.

98       The rapid degradation of GIP in plasma by dipeptidyl peptidase-4 (DPP-4) precludes  
99 to its use as a therapeutic approach. As such, a series of GIP modifications have previously  
100 been conducted and led to several GIP analogues with proven efficacy (Irwin and Flatt  
101 2009). From these manipulations, it appears that the N-terminal extremity of GIP, and  
102 particularly the first two amino acids, was particularly important in allowing receptor  
103 activation. Furthermore, only the first 30 amino acids are required to induce biological activity

(Hinke, et al. 2001). As such, we produced two new GIP analogues, namely [D-Ala<sup>2</sup>]-GIP<sub>1-30</sub> and [D-Ala<sup>2</sup>]-GIP-Tag that possess a D-alanine in position 2 to confer DPP-4 resistance. Furthermore, [D-Ala<sup>2</sup>]-GIP-Tag possesses a tag of 9 negatively charged amino acids at its C-terminal extremity that, according to previous published studies, should give a bone-specific affinity (Kasugai, et al. 2000; Yokogawa, et al. 2001). The current gold standard medication for treating post-menopausal osteoporosis is represented by bisphosphonates and as such, we thought to also ascertain how the two new molecules above compared with alendronate.

The main goals of this study were to (1) verify that the tag confers a bone-specific targeting, (2) ascertain the biological efficacy of these two new GIP analogues, [D-Ala<sup>2</sup>]-GIP<sub>1-30</sub> and [D-Ala<sup>2</sup>]-GIP-Tag and (3) investigate their therapeutic potentials in ovariectomy-induced bone fragility as compared to alendronate.

## 2. MATERIAL AND METHODS

### 2.1. Reagents

All GIP analogues were purchased from GeneCust Europe with a purity >95% (Dudelange, Luxembourg). Purity has been verified by high performance liquid chromatography and peptide composition validated by mass spectroscopy. Sequences are provided in table 1. Macrophage-colony stimulating factor (M-CSF) and receptor activator of nuclear factor κB ligand (RANKL) were purchased from R&D Systems Europe (Abingdon, UK). Fluo-4AM was purchased from Invitrogen (Carlsbad, CA, USA). All other chemicals were obtained from Sigma-Aldrich (Lyon, France) unless otherwise stated.

### 2.2. In vitro mineral binding assay

Carboxymethylated poly(2-hydroxyethylmethacrylate) (pHEMA) disks and their mineralization were performed as previously described (Filmon, et al. 2002). Mineralized disks were incubated for 16 h with 5 nmoles of 5-carboxyfluorescein (5-FAM), 5-FAM-[D-Ala<sup>2</sup>]-GIP<sub>1-30</sub>, 5-FAM-[D-Ala<sup>2</sup>]-GIP-Tag or calcein green. PHEMA disks were rinsed extensively with distilled water prior to observation with a Leica TCS SP8 confocal laser scanning microscope (Leica,

Nanterre, France). Excitation was performed at 488 nm with an argon laser and emission was recorded in the range 510-550 nm. After observation, the mineral was dissolved with 0.2M HCl overnight and fluorescence readings were performed with a M2 microplate reader (Molecular devices, St Gregoire, France) set up at 480 nm for excitation and 530 nm for emission. Calcium concentrations were estimated as published previously (Degeratu, et al. 2013).

### **2.3. Cell culture and activity of GIP analogues**

MC3T3-E1 cells were purchased from American type culture collection (ATCC, Teddington, UK). Cells were grown and expanded in propagation medium containing alpha minimum essential medium ( $\alpha$ MEM) supplemented with 5% fetal bovine serum (FBS), 5% bovine calf serum, 100 U/mL penicillin, and 100  $\mu$ g/mL streptomycin in a humidified atmosphere enriched with 5% CO<sub>2</sub> at 37°C.

Competitive whole cell binding studies were performed in cold  $\alpha$ MEM supplemented with 0.1% bovine serum albumin (BSA), protease inhibitors (Halt protease inhibitor cocktail, Thermofisher scientific, Villebon sur Yvette, France),  $8 \times 10^{-9}$ M FAM-GIP<sub>1-42</sub>, and appropriate peptide concentrations. Equilibrium binding was achieved overnight at 4°C. Cells were then washed twice with cold assay buffer, solubilized in 0.1M NaOH, and transferred to opaque microplate for fluorescence readings.

Cyclic adenosine monophosphate (cAMP) stimulation experiment was performed in response to 100 pM GIP analogues in MC3T3-E1 cells with a fluorometric commercially available kit (reference KGE002B, R&D Systems Europe) (Mieczkowska et al. 2015a). Assessment of the cell phospho-proteome was assessed with the Proteome profiler anti-phosphokinase assay (reference ARY003b, R&D Systems Europe).

MC3T3-E1 cells were seeded in 96-well plate with clear bottom and opaque edges (ibidi GmbH, Martinsried, Germany). Cells were incubated with 4  $\mu$ M Fluo-4-AM for 45 min at 37°C in the dark and washed with pre-warmed HEPES buffered saline. The plate was placed in a M2 microplate reader (Molecular devices) and signals were acquired at 37°C with an



excitation wavelength of 490 nm and an emission wavelength set at 515 nm for 5 min. Cells were then stimulated with 100 pM GIP analogues for 15 min and signals were again acquired with the microplate reader. Autofluorescence was measured in unloaded cells, and this value was subtracted from all measurements.

Collagen maturity assay was performed as described in detail elsewhere (Mieczkowska et al. 2015a).

In order to generate mature human osteoclasts, peripheral mononuclear blood cells were isolated from buffy coat (Etablissement français du sang, Angers, France) and cultured in the presence of 25 ng/ml M-CSF and 30 ng/ml soluble human RANKL as described previously (Mabilleau, et al. 2011).

## **2.4 Animals**

BALB/c (BALB/cJRj) mice were obtained from Janvier Labs (Saint-Berthevin, France). All animal experiments were approved by Ethical committee in animal use of the Pays de la Loire under the animal license CEEA-PdL06-01740.01. Mice were housed 4 animals per cage in the institutional animal lab (Agreement E49007002) at 24°C +/- 2°C with a 12-hour light/dark cycle, and were provided with tap water and normal diet (Diet A04, Safe, Augy, France) *ad libitum* until sacrifice by cervical dislocation. All procedures were conducted according to the French Animal Scientific Procedures Act 2013-118.

## **2.5. *In vivo* localization of fluorescently labelled GIP analogues**

Intraperitoneal injections of saline or fluorescent GIP analogues (50 nmoles/kg body weight) were performed at 4 weeks of age in 15 female BALB/c mice (n=5/group). This dose of fluorescent GIP analogues was chosen to ensure detection in the investigated tissues. Twenty-four hours after injection, visceral adipose tissue, adrenal gland, bladder, left femur and tibia, brain, heart, small intestine, kidney, liver, lung, pancreas, skeletal muscle, spleen and stomach were collected, immediately snap-frozen in liquid nitrogen and stored at -80°C until use. Then, frozen tissues were powdered, suspended in Tris 0.1M pH 7.4 and

fluorescence readings with a microplate reader as detailed above were performed. Fluorescence readings were normalized by the concentration of proteins measured with the bicinchoninic acid assay (Pierce Biotechnology, Rockford, IL). Right femurs of 4-week-old mice were collected at necropsy, fixed in buffered formalin and embedded in polymethylmethacrylate (pMMA) at low temperature (Chappard 2009). Thick cross-sections at the mid-diaphysis of all femurs were cut with a low speed precision saw (Minitom, Struers, Champigny sur Marne, France). Femur sections were grinded up to a thickness of 50  $\mu\text{m}$  and subsequently imaged with the confocal microscope as explained above. Additionally, right tibias of 5-FAM-[D-Ala<sup>2</sup>]-GIP-Tag-injected mice were collected at necropsy, fixed in buffered formalin and embedded in polymethylmethacrylate (pMMA) at low temperature. Thick cross-sections (500  $\mu\text{m}$ -thick) at the mid-diaphysis were cut with a low speed precision saw and incubated in saline or 0.1M acetic acid (pH 4.5) for 24 h. The resulting solution was buffered with 1M Tris and fluorescence readings were performed with the M2 microplate reader as explained above.

## **2.6. Long term effects of GIP analogues in ovariectomy-induced bone loss**

Bilateral ovariectomy (OVX) was performed in 32 BALB/c mice at 12 weeks of age under general anesthesia supplemented with a  $\beta 2$  adrenergic receptor agonist. At 16 weeks of age, mice were randomly allocated into four groups: vehicle daily (OVX+Veh, n=8), 25 nmoles/kg/day intraperitoneally (ip) [D-Ala<sup>2</sup>]-GIP<sub>1-30</sub> (OVX+GIP<sub>1-30</sub>, n=8), 25 nmoles/kg/day ip [D-Ala<sup>2</sup>]-GIP-Tag (OVX+GIP-Tag, n=8) and 10  $\mu\text{g}/\text{kg}$  alendronate twice a week ip (OVX+Aln, n=8). These doses and regimens of GIP analogues and alendronate were based on previous published studies where these molecules were proven active with beneficial effects on bone or equivalent to approved clinical dose (Mabilleau et al. 2014; Shao, et al. 2017). Eight sham-operated female BALB/c mice with the same age and injected daily with saline were used as controls (Sham+Veh). All mice from the second study were also administered with calcein (10 mg/kg; ip) 10 and 2 days before being culled at 24 weeks of age. At necropsy, blood was collected by intracardiac aspiration (~250 $\mu\text{l}$ ). Non-fasting glucose level were evaluated with

an Accu-Chek® mobile glucometer (Roche Diabetes Care GmbH, Mannheim, Germany). Then blood were spun at 13,000 rpm for 15 min at 4°C and serum was aliquoted, snap-frozen in liquid nitrogen and stored at -80°C until use. After necropsy, tibias, femurs and uterus were collected and cleaned of soft tissues. Femur length was measured with a digital caliper (Mitutoyo, Roissy en France, France).

## **2.7. ELISA**

Serum levels of C-terminal telopeptide of collagen type I (CTX-I) and N-terminal propeptide of type I collagen (P1NP) were measured with the RatLaps and Rat/mouse P1NP ELISA kits, respectively (Immunodiagnostic Systems Ltd, Boldon, UK), according to the manufacturer recommendations.

## **2.8. Microcomputed tomography**

X-ray microcomputed tomography (MicroCT) analyses of the abdomen were performed to measure abdominal fat volume, that represents a good indicator of whole body fat mass (Judex, et al. 2010). Anesthetized animals were placed in a Skyscan 1076 microtomograph (Bruker MicroCT, Kontich, Belgium) and the region localized between L1 and the hip was selected for fat depot evaluation. Acquisitions were performed at 40 kV, 250 µA, 100-ms integration time. The isotropic pixel size was fixed at 35 µm, the rotation step at 0.6° and exposure was done with a 0.5-mm aluminum filter. Tibias were scanned with a Skyscan 1172 microtomograph (Bruker MicroCT) operated at 70 kV, 100 µA, 340-ms integration time. The isotropic pixel size was fixed at 4 µm, the rotation step at 0.25° and exposure was done with a 0.5-mm aluminium filter. Each 3D reconstruction image dataset was binarized using global thresholding. Cortical volume of interest extended on 1-mm centered at the midshaft tibia. All histomorphometrical parameters were determined according to guidelines and nomenclature proposed by the American Society for Bone and Mineral Research (Bouxsein, et al. 2010).

## **2.9. Marrow adipose tissue assessment**

After microCT scans, tibias were embedded undecalcified in pMMA at 4°C. Longitudinal sections were cut and stained with toluidine blue. The extent of marrow adipose tissue (Ad.Ar/Ma.Ar) was computerized with a routine in Image J (release 1.51s, National Institutes of Health, Bethesda, MA). The nomenclature proposed by the American Society for Bone and Mineral Research was used in this study (Dempster, et al. 2013).

## **2.10. Bone strength assessment**

At necropsy, femurs were cleaned of soft tissue and immediately frozen in a saline-soaked gauze at -20°C. Three-point bending experiments were performed on femurs after thawing bones at 4°C overnight. Measurements were done with an Instron 5942 (Instron, Elancourt, France) as reported previously (Mieczkowska et al. 2015b). The load-displacement curve was acquired with the Bluehill 3 software (Instron). Ultimate load, ultimate displacement, stiffness and total absorbed energy were computerized (Turner and Burr 1993).

After three-point bending experiments, femurs were embedded undecalcified in pMMA at 4°C and cross-sections were made at the midshaft using a diamond saw (Accutom, Struers, Champigny sur Marne, France). Blocks were polished to a 1- $\mu$ m finish with diamond particles (Struers, France) and subjected to rehydration in saline 24h prior to nanoindentation testing. Twelve indentations, at distance from canals, osteocyte lacunae and/or microcracks were randomly positioned in cortical bone with a NHT-TTX system (Anton Paar, Les Ulis, France) as previously detailed (Aguado, et al. 2017). At maximum load, a holding period of 15 seconds was applied to avoid creeping of the bone material. The following material properties at the tissue-level: maximum load (Force max), indentation modulus ( $E_{IT}$ ), indentation hardness ( $H_{IT}$ ) and dissipated energy ( $W_{plast}$ ), were determined according to Oliver and Pharr (Oliver and Pharr 1992).

## **2.11. Fourier-transform infrared microscopy (FTIRM)**

Four micrometers cross-sectional sections of the midshaft femur were sandwiched between BaF<sub>2</sub> optical windows and FTIRM assessment was performed at bone formation site by

recording infrared spectra only between double calcein labeling. A Bruker Vertex 70 spectrometer (Bruker optics, Ettlingen, Germany) interfaced with a Bruker Hyperion 3000 infrared microscope were used as previously reported (Pereira, et al. 2017). Each spectrum was corrected for Mie scattering with the RMieS-EMSC\_v5 algorithm (kind gift of Prof Peter Gardner, University of Manchester, UK) prior to be subjected to pMMA subtraction. Second derivative spectroscopy was applied to find the position of underlying peaks and curve fitting was performed with a routine script in Matlab (The Mathworks, Natick, USA) as previously reported (Mansur et al. 2015). The evaluated infrared spectral parameters were (1) mineral-to-matrix ratio, calculated as the ratio of integrated areas of the  $\nu_1$ ,  $\nu_3$  phosphate band at 900-1200  $\text{cm}^{-1}$  to the amide I band at 1585-1725  $\text{cm}^{-1}$  (Boskey, et al. 2005); (2) mineral maturity calculated as the area ratio of the subbands at 1020  $\text{cm}^{-1}$  and 1030  $\text{cm}^{-1}$  of the phosphate band (Gadaleta, et al. 1996); (3) carbonate-to-phosphate ratio, calculated as the ratio of the  $\nu_2$  carbonate band at 850-900  $\text{cm}^{-1}$  to the  $\nu_1, \nu_3$  phosphate band (Paschalis, et al. 1996); (4) carbonate substitution type by integrating the area of subbands located at 866  $\text{cm}^{-1}$  (labile), 871  $\text{cm}^{-1}$  (type B) and 878  $\text{cm}^{-1}$  (type A) over the  $\nu_2$  carbonate band (Rey, et al. 1989); (5) acid phosphate content, calculated as the area ratio of the 1127  $\text{cm}^{-1}$  and 1096  $\text{cm}^{-1}$  subbands (Spevak, et al. 2013) and (6) collagen maturity, determined as the relative ratio of subbands located at 1660  $\text{cm}^{-1}$  (trivalent cross-links) and 1690  $\text{cm}^{-1}$  (divalent cross-links) of the amide I peak (Paschalis, et al. 2001).

## **2.12. Bone mineral density distribution (BMDD) evaluation**

Quantitative backscattered electron imaging (qBEI) experiments were performed on the same blocks and same regions as nanoindentation. A full description of qBEI preparation, calibration and analysis has already been extensively described elsewhere (Mabilleau et al. 2013; Mieczkowska et al. 2015b; Roschger, et al. 1998). Cortical bone area was imaged at a 200 X nominal magnification, corresponding to a pixel size of 0.5  $\mu\text{m}$ . Four images per samples were taken. Two variables were obtained from the bone mineral density distribution:

$Ca_{mean}$  as the average calcium concentration and  $Ca_{width}$  as the width of the histogram at half maximum of the peak. Following this, the blocks were imaged at a 200 X magnification with a confocal microscope (Leica SP8, Leica, Nanterre, France) equipped with an argon laser at 488 nm and a hybrid GaAs detector (Leica) to find bone surface with double labels. Confocal images were superimposed on qBEI images in order to delineate new bone matrix formed during the time-course of the study. Using ImageJ 1.51s, a straight line (4 pixel width) perpendicular to the mineralization front across the new bone structural unit with a step size of 0.5 $\mu$ m was drawn on qBEI image. The calcium content was plotted vs. distance of mineralization front. These plots show a biphasic aspect with fast mineralization process close to the mineralization front followed by a slow mineralization process. The two mineralization processes were then analysed by linear curve fitting with a lab-made routine in Excel 2010 (Microsoft, Issy-les-Moulineaux, France).  $Ca_{turn}$  was determined as the calcium concentration where the fast mineralization process was changing to the slow mineralization process as described by Roschger et al., (Roschger, et al. 2008)

### 2.13. Statistical analysis

All data were analyzed using Prism 6.0 (GraphPad Software Inc., La Jolla, CA). Mineral binding was analyzed by a one-way analysis of variance (ANOVA) followed by *post hoc* Dunnett's multiple comparisons tests. Tissue distribution of both fluorescent analogues was analyzed by a two-way ANOVA with Sidak's multiple comparisons tests. GIPr binding assay was analyzed by non-linear regression analysis. Intracellular signaling (cAMP, intracellular calcium and phospho-proteins) as well as in vitro collagen maturity and extent of osteoclast formation and resorption in vitro were analyzed with the non-parametrical Kruskal-Wallis test. Due to the adaptive nature of bone, bone strength, bone microarchitecture and bone compositional parameters have been adjusted for body size (body mass x femur length) using a linear regression method as reported in details elsewhere (Jepsen, et al. 2015). One-way ANOVA followed by *post hoc* Dunnett's multiple comparisons tests were employed to analyze differences between OVX+Veh and all the other groups of mice in any of the body

size-adjusted parameters. Differences at  $p$  equal to or less than 0.05 were considered significant.

### 3. RESULTS

#### 3.1. [D-Ala<sup>2</sup>]-GIP-Tag but not [D-Ala<sup>2</sup>]-GIP<sub>1-30</sub> is capable of binding to hydroxyapatite and targeting bone tissue

Microscopic examinations of calcospherites grown at the surface of carboxymethylated pHEMA revealed that 5-FAM-[D-Ala<sup>2</sup>]-GIP-Tag and calcein green, but neither 5-FAM-[D-Ala<sup>2</sup>]-GIP<sub>1-30</sub> nor 5-FAM alone, were significantly bound to hydroxyapatite (Figure 1A). Tissue distribution of the two fluorescently labeled analogues highlighted differences between the two molecules. Indeed, 5-FAM-[D-Ala<sup>2</sup>]-GIP<sub>1-30</sub> was mainly observed in adipose tissue, adrenal gland, bone, brain, intestine, liver and pancreas, whilst 5-FAM-[D-Ala<sup>2</sup>]-GIP-Tag was exclusively found in bone (Figure 1B). Microscopic examinations of femur midshaft cross-sections in 5-FAM-[D-Ala<sup>2</sup>]-GIP-Tag-injected mice revealed the presence of fluorescent bands, suggesting the incorporation of this analogue in the bone mineral (Figure 1C). On the other hand, such bone distribution was not observed in 5-FAM-[D-Ala<sup>2</sup>]-GIP<sub>1-30</sub>-injected animals (Figure 1C). Furthermore, incubation of thick tibia slices in acidic conditions (pH 4.5), but not in neutral solution, was capable of releasing 5-FAM-[D-Ala<sup>2</sup>]-GIP-Tag (Figure 1D).

#### 3.2. Cellular and molecular activities of [D-Ala<sup>2</sup>]-GIP-Tag are not affected by the C-terminal modification

Next, we thought to investigate the biological activity of both GIP analogues. As represented in Figure 2A, [D-Ala<sup>2</sup>]-GIP<sub>1-30</sub> and [D-Ala<sup>2</sup>]-GIP-Tag did not show any differences in their capacity to bind to the GIPr with IC<sub>50</sub> of 65.5±2.5 pM and 72.9±2.7 pM, respectively. More importantly, their binding activity was similar to GIP<sub>1-42</sub>, with IC<sub>50</sub> of 65.3±1.7 pM. Both GIP analogues were capable of inducing cAMP production and rise in intracellular calcium to the same level as observed with GIP<sub>1-42</sub> (Figure 2A). Phospho-proteome analysis showed that

osteoblasts stimulated with GIP<sub>1-42</sub> also activated p38 $\alpha$ , CREB, AMPK $\alpha$ 2 and STAT2 in addition to cAMP (Figure 2B). [D-Ala<sup>2</sup>]-GIP<sub>1-30</sub> and [D-Ala<sup>2</sup>]-GIP-Tag showed similar actions on all these intracellular pathways (Figure 2B). Finally, we tested whether [D-Ala<sup>2</sup>]-GIP<sub>1-30</sub> and [D-Ala<sup>2</sup>]-GIP-Tag were capable of improving collagen maturity as observed with GIP<sub>1-42</sub> and indeed, this parameter was significantly augmented by 32% and 37%, with [D-Ala<sup>2</sup>]-GIP<sub>1-30</sub> and [D-Ala<sup>2</sup>]-GIP-Tag, respectively as compared with untreated cells (Figure 2C). As suspected, both GIP analogues were also capable to reduce osteoclast formation and osteoclast-mediated bone resorption *in vitro* in a similar extent to GIP<sub>1-42</sub> (Figure 2D).

### 3.3. Effects of [D-Ala<sup>2</sup>]-GIP<sub>1-30</sub> vs. [D-Ala<sup>2</sup>]-GIP-Tag in OVX-induced bone loss

We next examined the biological effects of GIP analogues in the OVX mouse model. As compared with Sham+Veh animals and shown in Table 2, OVX+Veh mice presented with higher abdominal fat volume and CTx-I levels and lower uterus mass. Treatment with [D-Ala<sup>2</sup>]-GIP<sub>1-30</sub> significantly reduced CTx-I levels whilst treatment of OVX animals with [D-Ala<sup>2</sup>]-GIP-Tag significantly reduced abdominal fat volume, marrow adipose tissue and CTx-I levels. Alendronate administration only significantly reduced CTx-I levels.

After the 8-week experimental treatment period, structural mechanical properties were assessed by three-point bending (Figures 3 A-F). As expected, OVX+Veh mice presented with significant reductions in ultimate force (-18%,  $p=0.0005$ ), yield load (-27%,  $p<0.0001$ ) and stiffness (-34%,  $p<0.0001$ ). Treatments with alendronate or [D-Ala<sup>2</sup>]-GIP<sub>1-30</sub>, but not [D-Ala<sup>2</sup>]-GIP-Tag, significantly augmented by 33% ( $p<0.0001$ ) and 25% ( $p=0.0013$ ) stiffness, respectively. Bone strength was also investigated at the tissue level by nanoindentation (Figures 3 G-J). As compared with Sham animals, OVX+Veh mice presented no significant alterations in any of the studied parameters. The use of alendronate significantly augmented  $H_{IT}$  by 29% ( $p=0.0191$ ). Neither [D-Ala<sup>2</sup>]-GIP<sub>1-30</sub> nor [D-Ala<sup>2</sup>]-GIP-Tag significantly modified strength at the tissue level.

As compared with Sham+Veh animals, significant microarchitectural alterations of cortical bone were evidenced as expected in OVX+Veh animals and represented by lower total



cross-sectional area (Tt.Ar, -10%,  $p=0.0249$ ), marrow area (Ma.Ar, -14%,  $p=0.0046$ ) and cortical area (Ct.Ar, -9%,  $p=0.0248$ ) (Table 3). On the other hand, cortical thickness (Ct.Th), moment of inertia about the anteroposterior ( $I_{ap}$ ) or mediolateral ( $I_{ml}$ ) axis and polar moment of inertia (J) were not significantly different between the two groups of animals. As compared with OVX+Veh animals, treatment with [D-Ala<sup>2</sup>]-GIP<sub>1-30</sub> significantly increased Tt.Ar, Ma.Ar, Ct.Ar and J by 10% ( $p=0.0417$ ), 16% ( $p=0.0041$ ), 9% ( $p=0.0430$ ) and 18% ( $p=0.0246$ ), respectively. Treatment with [D-Ala<sup>2</sup>]-GIP-Tag did not result in significant modifications of cortical microarchitecture although a trend to similar effects as observed with [D-Ala<sup>2</sup>]-GIP<sub>1-30</sub> was noted (Table 3). Treatment with alendronate resulted only in lower values for  $I_{ml}$  (-21%,  $p=0.0277$ ).

Alterations of bone matrix composition was also evidenced in OVX+Veh animals as compared with Sham+Veh (Figure 4). Indeed, at site of bone formation, collagen maturity and mineral-to-matrix ratio were significantly lowered by 25% ( $p=0.0261$ ) and 35% ( $p=0.0070$ ), respectively in OVX+Veh animals. As compared with OVX+Veh animals, treatment with [D-Ala<sup>2</sup>]-GIP<sub>1-30</sub> or [D-Ala<sup>2</sup>]-GIP-Tag significantly lowered the overall mean calcium distribution in the bone matrix ( $Ca_{mean}$ ) by 7% ( $p=0.0002$ ) and 4% ( $p=0.0217$ ), respectively. These two molecules also reduced the  $Ca_{turn}$  value by 6% ( $p=0.005$ ) and 7% ( $p=0.002$ ), respectively. At site of bone formation, none of these molecules modified the bone matrix composition. On the other hand, treatment with alendronate significantly reduced calcium distribution heterogeneity ( $Ca_{width}$ ) by 11% ( $p=0.0044$ ) and augmented  $Ca_{turn}$  values by 7% ( $p<0.001$ ) in the bone matrix. At site of bone formation, alendronate resulted in higher carbonate-to-phosphate ratio by 16% ( $p=0.0204$ ), mainly by reduction in loosely bound carbonate (-47%,  $p=0.0053$ ) and increase in type B carbonate substitution (31%,  $p=0.0008$ ).

#### 4. DISCUSSION

With respect to its important role in maintaining bone strength in animal models of receptor deletion, GIP has promises as a therapeutic agent in treating bone fragility. In the present study, we investigated bone-targeting capacities and biological activities as well as

therapeutical potencies of two new GIP analogues in ovariectomy-induced bone loss. The bone-targeting capacity of [D-Ala<sup>2</sup>]-GIP-Tag, as opposed to [D-Ala<sup>2</sup>]-GIP<sub>1-30</sub>, was evident and emphasized the importance of acidic amino acids in promoting bone affinity. Acidic amino acid tag mimics the observed aspartic acid repetition in the noncollagenous bone protein osteopontin. In bone, after secretion, osteopontin rapidly binds to hydroxyapatite and sequence analysis of osteopontin identified the aspartic acid repetition as a putative mineral-binding site (Butler 1989; Oldberg, et al. 1986). Similarly to what is observed with bisphosphonate, a molecule bound to the bone mineral is thought to be released upon bone resorption. The first evidence suggesting such properties of the acidic amino acid tag was reported by Kasugai and coworkers in 2000 (Kasugai et al. 2000). Since their discovery, at least six distinct molecules have been developed so far with bone-targeting properties using an acidic amino acid tag (Hsieh, et al. 2014; Miller, et al. 2008; Montano, et al. 2008; Nishioka, et al. 2006; Takahashi, et al. 2008; Yokogawa et al. 2001). In 2007, Murphy et al. reported the higher efficacy of acidic amino acid tags in comparison to the bisphosphonate structural group (Murphy, et al. 2007). We deliberately chose to fuse this tag at the C-terminal end of [D-Ala<sup>2</sup>]-GIP<sub>1-30</sub> because only the first 30 amino acids are important for GIP helicoïdal secondary structure and hence its receptor binding and biological properties (Alana, et al. 2006; Manhart, et al. 2003). However, in this study, we also provided clear evidences that [D-Ala<sup>2</sup>]-GIP<sub>1-30</sub> and [D-Ala<sup>2</sup>]-GIP-Tag presented the same receptor binding affinities as full length GIP<sub>1-42</sub> and that the same intracellular signaling pathways were activated in osteoblasts in response to these GIP analogues. Previously GIP<sub>1-42</sub> has been reported to enhance collagen maturity in osteoblast cultures (Mieczkowska et al. 2015a) and to reduce cell differentiation and activity in osteoclast cultures (Mabilleau et al. 2016). In the present study, we provided clear evidences that the two new GIP analogues, [D-Ala<sup>2</sup>]-GIP<sub>1-30</sub> and [D-Ala<sup>2</sup>]-GIP-Tag, exhibited similar actions in osteoblast and osteoclast cultures. However, when administered *in vivo*, these two molecules presented differences. Indeed, [D-Ala<sup>2</sup>]-GIP<sub>1-30</sub> localizes in several tissues that could potentially affect bone physiology whilst as discussed above, [D-Ala<sup>2</sup>]-GIP-Tag localizes almost exclusively in bone. In the ovariectomy-

induced bone fragility model, [D-Ala<sup>2</sup>]-GIP<sub>1-30</sub>, but not [D-Ala<sup>2</sup>]-GIP-Tag, was proven potent to improve bone strength, mainly by modifying the cortical microarchitecture. However, caution should be taken for interpretation of these observations. Firstly, the activity of [D-Ala<sup>2</sup>]-GIP-Tag has been tested in isolated cell culture, but not in vivo after incorporation into the bone mineral. Our release assay demonstrated that at acidic pH, close to pH obtained during osteoclast resorption, the fluorescent peptide could be released from bone. However, it was not possible to assess its biological activity. Furthermore, due to the low concentration given to the animals, it was not possible to assess the presence of [D-Ala<sup>2</sup>]-GIP-Tag in blood or urine. As such, we cannot rule out that the observed lack of effects of [D-Ala<sup>2</sup>]-GIP-Tag could be due to either low bioavailability or degradation of the peptide after osteoclast resorption. Another explanation, and in addition to GIPr tissue targeting, could suggest that to be beneficial for bone health, extraskelatal GIPr have to be targeted rather than bone-specific GIPr. However, a limitation to this study is that we did not generate tissue-specific invalidation or extraskelatal tissue specific activation of GIPr to ascertain how the GIP/GIPr pathway controls bone physiology.

The mechanism of action of [D-Ala<sup>2</sup>]-GIP<sub>1-30</sub> was also compared with alendronate. In the present study, alendronate, given at a dose comparable to what is used in humans in the treatment of post-menopausal osteoporosis (i.e. 70 mg/week orally), improved bone strength by acting mostly on bone matrix composition (H<sub>IT</sub>, Ca<sub>width</sub>, carbonate-to-phosphate ratio) rather than restoring cortical bone microarchitecture. On the other hand, [D-Ala<sup>2</sup>]-GIP<sub>1-30</sub> acted preferentially on cortical bone microarchitecture and had almost no action on bone matrix composition, except a small decrease in tissue mineral density. This indicates that the molecular mechanisms of action of these two pharmacological interventions are probably different and in the future, administration of both molecules jointly should be envisaged.

In conclusion, we developed two new GIP analogues that target whole-body GIPr or only bone-specific GIPr. In ovariectomized animals, only [D-Ala<sup>2</sup>]-GIP<sub>1-30</sub> was potent in ameliorating bone strength by restoring cortical bone microarchitecture rather than acting on bone matrix composition in opposition to what was observed with alendronate. This study

brought new evidences that targeting the GIP/GIPr pathway might be valuable in bone disorders although further studies will be needed before translating these findings to human post-menopausal osteoporosis.

## 5. DECLARATION OF INTEREST

None of the authors has any conflict of interest to report

## 6. FUNDING

This work was supported by a grant from the Société Française de Rhumatologie.

## 7. AUTHOR CONTRIBUTIONS

**Guillaume Mabileau:** Conception and Design, acquisition of data, analysis and interpretation of data, drafting and revising the manuscript

**Benoit Gobron:** acquisition of data, analysis and interpretation of data, revising the manuscript

**Aleksandra Mieczkowska:** acquisition of data, analysis and interpretation of data, revising the manuscript

**Rodolphe Perrot:** acquisition of data, analysis and interpretation of data, revising the manuscript

**Daniel Chappard:** Analysis and interpretation of data, revising the manuscript

All authors approved the current version of the manuscript. Guillaume Mabileau takes responsibility for the integrity of the data and analysis.

## 8. ACKNOWLEDGEMENTS

The authors are grateful to Nadine Gaborit and Stéphanie Lemièrre for their help with microCT. The authors also thank the personnel of the animal care facility (University of Angers-SCAHU) for their help with animal handling and injection.

## 9. REFERENCES

- Aguado E, Mabilieu G, Goyenvalle E & Chappard D 2017 Hypodynamia Alters Bone Quality and Trabecular Microarchitecture. *Calcif Tissue Int* **100** 332-340.
- Alana I, Parker JC, Gault VA, Flatt PR, O'Harte FP, Malthouse JP & Hewage CM 2006 NMR and alanine scan studies of glucose-dependent insulinotropic polypeptide in water. *J Biol Chem* **281** 16370-16376.
- Baggio LL & Drucker DJ 2007 Biology of incretins: GLP-1 and GIP. *Gastroenterology* **132** 2131-2157.
- Bollag RJ, Zhong Q, Phillips P, Min L, Zhong L, Cameron R, Mulloy AL, Rasmussen H, Qin F, Ding KH, et al. 2000 Osteoblast-derived cells express functional glucose-dependent insulinotropic peptide receptors. *Endocrinology* **141** 1228-1235.
- Boskey AL, DiCarlo E, Paschalis E, West P & Mendelsohn R 2005 Comparison of mineral quality and quantity in iliac crest biopsies from high- and low-turnover osteoporosis: an FT-IR microspectroscopic investigation. *Osteoporos Int* **16** 2031-2038.
- Bouxsein ML, Boyd SK, Christiansen BA, Guldberg RE, Jepsen KJ & Muller R 2010 Guidelines for assessment of bone microstructure in rodents using micro-computed tomography. *J Bone Miner Res* **25** 1468-1486.
- Butler WT 1989 The nature and significance of osteopontin. *Connect Tissue Res* **23** 123-136.
- Chappard D 2009 Technical aspects: how do we best prepare bone samples for proper histological analysis? In *Bone cancer: progression and therapeutic approaches*, pp 203-210. Ed D Heymann. London: Academic press Elsevier.
- Degeratu CN, Mabilieu G, Cincu C & Chappard D 2013 Aluminum inhibits the growth of hydroxyapatite crystals developed on a biomimetic methacrylic polymer. *J Trace Elem Med Biol* **27** 346-351.
- Dempster DW, Compston JE, Drezner MK, Glorieux FH, Kanis JA, Malluche H, Meunier PJ, Ott SM, Recker RR & Parfitt AM 2013 Standardized nomenclature, symbols, and units for

bone histomorphometry: a 2012 update of the report of the ASBMR Histomorphometry Nomenclature Committee. *J Bone Miner Res* **28** 2-17.

Filmon R, Grizon F, Basle MF & Chappard D 2002 Effects of negatively charged groups (carboxymethyl) on the calcification of poly(2-hydroxyethyl methacrylate). *Biomaterials* **23** 3053-3059.

Gadaleta SJ, Paschalis EP, Betts F, Mendelsohn R & Boskey AL 1996 Fourier transform infrared spectroscopy of the solution-mediated conversion of amorphous calcium phosphate to hydroxyapatite: new correlations between X-ray diffraction and infrared data. *Calcif Tissue Int* **58** 9-16.

Gaudin-Audrain C, Irwin N, Mansur S, Flatt PR, Thorens B, Basle M, Chappard D & Mabileau G 2013 Glucose-dependent insulintropic polypeptide receptor deficiency leads to modifications of trabecular bone volume and quality in mice. *Bone* **53** 221-230.

Henriksen DB, Alexandersen P, Bjarnason NH, Vilsboll T, Hartmann B, Henriksen EE, Byrjalsen I, Krarup T, Holst JJ & Christiansen C 2003 Role of gastrointestinal hormones in postprandial reduction of bone resorption. *J Bone Miner Res* **18** 2180-2189.

Hinke SA, Manhart S, Pamir N, Demuth H, R WG, Pederson RA & McIntosh CH 2001 Identification of a bioactive domain in the amino-terminus of glucose-dependent insulintropic polypeptide (GIP). *Biochim Biophys Acta* **1547** 143-155.

Hsieh KC, Kao CL, Feng CW, Wen ZH, Chang HF, Chuang SC, Wang GJ, Ho ML, Wu SM, Chang JK, et al. 2014 A novel anabolic agent: a simvastatin analogue without HMG-CoA reductase inhibitory activity. *Org Lett* **16** 4376-4379.

Irwin N & Flatt PR 2009 Therapeutic potential for GIP receptor agonists and antagonists. *Best Pract Res Clin Endocrinol Metab* **23** 499-512.

Jepsen KJ, Silva MJ, Vashishth D, Guo XE & van der Meulen MC 2015 Establishing biomechanical mechanisms in mouse models: practical guidelines for systematically evaluating phenotypic changes in the diaphyses of long bones. *J Bone Miner Res* **30** 951-966.

549 Judex S, Luu YK, Ozcivici E, Adler B, Lublinsky S & Rubin CT 2010 Quantification of  
 550 adiposity in small rodents using micro-CT. *Methods* **50** 14-19.  
 551 Kasugai S, Fujisawa R, Waki Y, Miyamoto K & Ohya K 2000 Selective drug delivery system  
 552 to bone: small peptide (Asp)<sup>6</sup> conjugation. *J Bone Miner Res* **15** 936-943.  
 553 Mabileau G, Chappard D & Sabokbar A 2011 Role of the A20-TRAF6 axis in  
 554 lipopolysaccharide-mediated osteoclastogenesis. *J Biol Chem* **286** 3242-3249.  
 555 Mabileau G, Mieczkowska A, Irwin N, Flatt PR & Chappard D 2013 Optimal bone  
 556 mechanical and material properties require a functional glucagon-like peptide-1 receptor. *J*  
 557 *Endocrinol* **219** 59-68.  
 558 Mabileau G, Mieczkowska A, Irwin N, Simon Y, Audran M, Flatt PR & Chappard D 2014  
 559 Beneficial effects of a N-terminally modified GIP agonist on tissue-level bone material  
 560 properties. *Bone* **63** 61-68.  
 561 Mabileau G, Perrot R, Mieczkowska A, Boni S, Flatt PR, Irwin N & Chappard D 2016  
 562 Glucose-dependent insulintropic polypeptide (GIP) dose-dependently reduces osteoclast  
 563 differentiation and resorption. *Bone* **91** 102-112.  
 564 Manhart S, Hinke SA, McIntosh CH, Pederson RA & Demuth HU 2003 Structure-function  
 565 analysis of a series of novel GIP analogues containing different helical length linkers.  
 566 *Biochemistry* **42** 3081-3088.  
 567 Mansur SA, Mieczkowska A, Bouvard B, Flatt PR, Chappard D, Irwin N & Mabileau G 2015  
 568 Stable Incretin Mimetics Counter Rapid Deterioration of Bone Quality in Type 1 Diabetes  
 569 Mellitus. *J Cell Physiol* **230** 3009-3018.  
 570 Mansur SA, Mieczkowska A, Flatt PR, Bouvard B, Chappard D, Irwin N & Mabileau G 2016  
 571 A new stable GIP-Oxyntomodulin hybrid peptide improved bone strength both at the organ  
 572 and tissue levels in genetically-inherited type 2 diabetes mellitus. *Bone* **87** 102-113.  
 573 Mieczkowska A, Bouvard B, Chappard D & Mabileau G 2015a Glucose-dependent  
 574 insulintropic polypeptide (GIP) directly affects collagen fibril diameter and collagen cross-  
 575 linking in osteoblast cultures. *Bone* **74** 29-36.

576 Mieczkowska A, Irwin N, Flatt PR, Chappard D & Mabileau G 2013 Glucose-dependent  
 577 insulintropic polypeptide (GIP) receptor deletion leads to reduced bone strength and quality.  
 578 *Bone* **56** 337-342.

579 Mieczkowska A, Mansur S, Bouvard B, Flatt PR, Thorens B, Irwin N, Chappard D &  
 580 Mabileau G 2015b Double incretin receptor knock-out (DIRKO) mice present with alterations  
 581 of trabecular and cortical micromorphology and bone strength. *Osteoporos Int* **26** 209-218.

582 Miller SC, Pan H, Wang D, Bowman BM, Kopeckova P & Kopecek J 2008 Feasibility of using  
 583 a bone-targeted, macromolecular delivery system coupled with prostaglandin E(1) to  
 584 promote bone formation in aged, estrogen-deficient rats. *Pharm Res* **25** 2889-2895.

585 Montano AM, Oikawa H, Tomatsu S, Nishioka T, Vogler C, Gutierrez MA, Oguma T, Tan Y,  
 586 Grubb JH, Dung VC, et al. 2008 Acidic amino acid tag enhances response to enzyme  
 587 replacement in mucopolysaccharidosis type VII mice. *Mol Genet Metab* **94** 178-189.

588 Murphy MB, Hartgerink JD, Goepferich A & Mikos AG 2007 Synthesis and in vitro  
 589 hydroxyapatite binding of peptides conjugated to calcium-binding moieties.  
 590 *Biomacromolecules* **8** 2237-2243.

591 Nishioka T, Tomatsu S, Gutierrez MA, Miyamoto K, Trandafirescu GG, Lopez PL, Grubb JH,  
 592 Kanai R, Kobayashi H, Yamaguchi S, et al. 2006 Enhancement of drug delivery to bone:  
 593 characterization of human tissue-nonspecific alkaline phosphatase tagged with an acidic  
 594 oligopeptide. *Mol Genet Metab* **88** 244-255.

595 Nissen A, Christensen M, Knop FK, Vilsboll T, Holst JJ & Hartmann B 2014 Glucose-  
 596 dependent insulintropic polypeptide inhibits bone resorption in humans. *J Clin Endocrinol*  
 597 *Metab* **99** E2325-2329.

598 Oldberg A, Franzen A & Heinegard D 1986 Cloning and sequence analysis of rat bone  
 599 sialoprotein (osteopontin) cDNA reveals an Arg-Gly-Asp cell-binding sequence. *Proc Natl*  
 600 *Acad Sci U S A* **83** 8819-8823.

601 Oliver WC & Pharr GM 1992 An improved technique for determining hardness and elastic  
 602 modulus using load and displacement sensing indentation experiments. *J Mater Res* **7** 1564-  
 603 1583.



- 604 Paschalis EP, DiCarlo E, Betts F, Sherman P, Mendelsohn R & Boskey AL 1996 FTIR  
605 microspectroscopic analysis of human osteonal bone. *Calcif Tissue Int* **59** 480-487.
- 606 Paschalis EP, Verdelis K, Doty SB, Boskey AL, Mendelsohn R & Yamauchi M 2001  
607 Spectroscopic characterization of collagen cross-links in bone. *J Bone Miner Res* **16** 1821-  
608 1828.
- 609 Pereira M, Gohin S, Roux JP, Fisher A, Cleasby ME, Mabileau G & Chenu C 2017  
610 Exenatide Improves Bone Quality in a Murine Model of Genetically Inherited Type 2 Diabetes  
611 Mellitus. *Front Endocrinol (Lausanne)* **8** 327.
- 612 Rey C, Collins B, Goehl T, Dickson IR & Glimcher MJ 1989 The carbonate environment in  
613 bone mineral: a resolution-enhanced Fourier Transform Infrared Spectroscopy Study. *Calcif*  
614 *Tissue Int* **45** 157-164.
- 615 Roschger P, Fratzl P, Eschberger J & Klaushofer K 1998 Validation of quantitative  
616 backscattered electron imaging for the measurement of mineral density distribution in human  
617 bone biopsies. *Bone* **23** 319-326.
- 618 Roschger P, Paschalis EP, Fratzl P & Klaushofer K 2008 Bone mineralization density  
619 distribution in health and disease. *Bone* **42** 456-466.
- 620 Shao Y, Hernandez-Buquer S, Childress P, Stayrook KR, Alvarez MB, Davis H, Plotkin LI,  
621 He Y, Condon KW, Burr DB, et al. 2017 Improving Combination Osteoporosis Therapy in a  
622 Preclinical Model of Heightened Osteoanabolism. *Endocrinology* **158** 2722-2740.
- 623 Spevak L, Flach CR, Hunter T, Mendelsohn R & Boskey A 2013 Fourier transform infrared  
624 spectroscopic imaging parameters describing acid phosphate substitution in biologic  
625 hydroxyapatite. *Calcif Tissue Int* **92** 418-428.
- 626 Takahashi T, Yokogawa K, Sakura N, Nomura M, Kobayashi S & Miyamoto K 2008 Bone-  
627 targeting of quinolones conjugated with an acidic oligopeptide. *Pharm Res* **25** 2881-2888.
- 628 Torekov SS, Harslof T, Rejnmark L, Eiken P, Jensen JB, Herman AP, Hansen T, Pedersen  
629 O, Holst JJ & Langdahl BL 2014 A functional amino acid substitution in the glucose-  
630 dependent insulinotropic polypeptide receptor (GIPR) gene is associated with lower bone  
631 mineral density and increased fracture risk. *J Clin Endocrinol Metab* **99** E729-733.

632 Tsukiyama K, Yamada Y, Yamada C, Harada N, Kawasaki Y, Ogura M, Bessho K, Li M,  
633 Amizuka N, Sato M, et al. 2006 Gastric inhibitory polypeptide as an endogenous factor  
634 promoting new bone formation after food ingestion. *Mol Endocrinol* **20** 1644-1651.  
635 Turner CH & Burr DB 1993 Basic biomechanical measurements of bone: a tutorial. *Bone* **14**  
636 595-608.  
637 Walsh JS & Henriksen DB 2010 Feeding and bone. *Arch Biochem Biophys* **503** 11-19.  
638 Xie D, Cheng H, Hamrick M, Zhong Q, Ding KH, Correa D, Williams S, Mulloy A, Bollag W,  
639 Bollag RJ, et al. 2005 Glucose-dependent insulintropic polypeptide receptor knockout mice  
640 have altered bone turnover. *Bone* **37** 759-769.  
641 Yokogawa K, Miya K, Sekido T, Higashi Y, Nomura M, Fujisawa R, Morito K, Masamune Y,  
642 Waki Y, Kasugai S, et al. 2001 Selective delivery of estradiol to bone by aspartic acid  
643 oligopeptide and its effects on ovariectomized mice. *Endocrinology* **142** 1228-1233.  
644

## FIGURE LEGENDS

**Figure 1: Mineral-binding capacity of GIP analogues.** (A) 5-FAM-[D-Ala<sup>2</sup>]-GIP-Tag and 5-FAM-[D-Ala<sup>2</sup>]-GIP<sub>1-30</sub> were incubated for 24h with disks of pHEMA that had been previously mineralized. 5-FAM and Calcein were used as negative and positive controls, respectively. 5-FAM-[D-Ala<sup>2</sup>]-GIP-Tag but not 5-FAM-[D-Ala<sup>2</sup>]-GIP<sub>1-30</sub> was capable of significantly binding to the mineralized disks. Values are means  $\pm$  SEM. #:  $p < 0.05$  vs. 5-FAM. (B) Tissue distribution of 5-FAM, 5-FAM-[D-Ala<sup>2</sup>]-GIP<sub>1-30</sub> and 5-FAM-[D-Ala<sup>2</sup>]-GIP-Tag. Fluorescence, in arbitrary units (a.u.) was weighted by the protein mass and detected in several tissues harvested from animals injected with 5-FAM-[D-Ala<sup>2</sup>]-GIP<sub>1-30</sub>. On the other hand, fluorescence due to 5-FAM-[D-Ala<sup>2</sup>]-GIP-Tag was exclusively found in bone. \*:  $p < 0.05$  vs. 5-FAM, #:  $p < 0.05$  vs. 5-FAM-[D-Ala<sup>2</sup>]-GIP<sub>1-30</sub>. Values are means  $\pm$  SEM. (C) 5-FAM-[D-Ala<sup>2</sup>]-GIP<sub>1-30</sub> and 5-FAM-[D-Ala<sup>2</sup>]-GIP-Tag were injected into young mice and the extent of GIP analogue binding in bone was assessed after 16h. A significant fluorescent line was clearly visible in the bone matrix of animals injected with 5-FAM-[D-Ala<sup>2</sup>]-GIP-Tag but not in animals injected with 5-FAM-[D-Ala<sup>2</sup>]-GIP<sub>1-30</sub>. Arrowheads indicate the fluorescence line. CtB: cortical bone, BM: bone marrow. (D) [D-Ala<sup>2</sup>]-GIP-Tag at acidic but not neutral pH was released from the bone slice as demonstrated by significant higher level of fluorescence. \*:  $p < 0.05$  vs. pH 7.0. Values are means  $\pm$  SEM.

**Figure 2: Biological activity of GIP analogues.** (A) Receptor binding properties and activation of cAMP and intracellular calcium. Receptor binding properties, cAMP and intracellular calcium responses of [D-Ala<sup>2</sup>]-GIP<sub>1-30</sub> and [D-Ala<sup>2</sup>]-GIP-Tag were not significantly different to those of native GIP<sub>1-42</sub>. Values are means  $\pm$  SEM. (B) Activation of intracellular pathways in MC3T3-E1 cells. [D-Ala<sup>2</sup>]-GIP<sub>1-30</sub>, [D-Ala<sup>2</sup>]-GIP-Tag and GIP<sub>1-42</sub> significantly increased the phosphorylation of p38 $\alpha$ , CREB, AMPK $\alpha$ 2 and STAT2 in a similar manner. \*:  $p < 0.05$  vs. vehicle. Values are means  $\pm$  SEM. (C) [D-Ala<sup>2</sup>]-GIP<sub>1-30</sub>, [D-Ala<sup>2</sup>]-GIP-Tag and

GIP<sub>1-42</sub> significantly increased collagen maturity *in vitro* and (D) reduced the number of newly generated osteoclast per well and the extent of osteoclast resorption. Values are means  $\pm$  SEM. \*:  $p < 0.05$  vs. vehicle and #:  $p < 0.05$  vs. M-CSF+RANKL.

30

**Figure 3: Effects of GIP analogues on bone strength in ovariectomy-induced bone loss.** (A-F) Bone strength has been assessed at the whole body-level by three point bending and (G-J) at the tissue level by nanoindentation. Values are means  $\pm$  SEM.  $H_{IT}$ : indentation hardness,  $E_{IT}$ : indentation modulus, Force max: Maximum load to reach 900 nm in depth,  $W_{plast}$ : Dissipated energy. \*:  $p < 0.05$  vs. OVX+Veh.

36

**Figure 4: Effects of GIP analogues on bone matrix composition.** (A) Tissue mineral density distribution has been studied by qBEI at the midshaft tibia and revealed significant lower values of  $Ca_{mean}$  and  $Ca_{turn}$  in the presence of [D-Ala<sup>2</sup>]-GIP<sub>1-30</sub> or [D-Ala<sup>2</sup>]-GIP-Tag and a significant lower heterogeneity and higher  $Ca_{turn}$  in the presence of alendronate. Values are means  $\pm$  SEM. \*:  $p < 0.05$  vs. OVX+Veh. (B) Bone matrix composition has been investigated at site of bone formation and revealed the lack of effects of both GIP analogues. Treatment with alendronate resulted in higher values for carbonate-to-phosphate ratio and type B carbonate substitution and a lower value of labile carbonate substitution. Values are means  $\pm$  SEM. \*:  $p < 0.05$  vs. OVX+Veh.

46

## 9. TABLES

**Table 1. Peptide sequences and characteristics**

GIP analogues	Amino acid sequence	Purity	Theoretical molecular weight (Da)	Measured molecular weight (Da)
GIP <sub>1-42</sub>	Y[D-Ala]EGTFISDYSIAMDKIHQQDFVNWLLAQKGKKNDWKHNITQ	96.5%	4983.53	4983.64
[D-Ala <sup>2</sup> ]-GIP <sub>1-30</sub>	Y[D-Ala]EGTFISDYSIAMDKIHQQDFVNWLLAQK	97.9%	3531.95	3532.02
5-FAM-[D-Ala <sup>2</sup> ]-GIP <sub>1-30</sub>	5'Fam-Y[D-Ala]EGTFISDYSIAMDKIHQQDFVNWLLAQK	96.9%	3890.25	3890.34
[D-Ala <sup>2</sup> ]GIP-Tag	Y[D-Ala]EGTFISDYSIAMDKIHQQDFVNWLLAQKGAADDDDDD	95.8%	4421.68	4421.76
5-FAM-[D-Ala <sup>2</sup> ]GIP-Tag	5'Fam- Y[D-Ala]EGTFISDYSIAMDKIHQQDFVNWLLAQKGAADDDDDD	95.6%	4779.98	4780.08

**Table 2. Body weight, composition and metabolic properties.**

	Sham+Veh	OVX+Veh	OVX+GIP <sub>1-30</sub>	OVX+GIP-Tag	OVX+Aln
Body mass (g)	23.5 ± 0.4 (0.062)	25.6 ± 0.9	26.1 ± 0.5 (0.945)	23.3 ± 0.6 (0.053)	26.6 ± 0.6 (0.645)
Abdominal fat volume (%)	14.6 ± 0.6 (<0.001)	24.7 ± 2.4	23.1 ± 1.6 (0.695)	10.8 ± 1.0 (<0.001)	25.6 ± 1.8 (0.695)
Uterus mass (g)	0.14 ± 0.01 (<0.001)	0.04 ± 0.01	0.05 ± 0.01 (0.915)	0.03 ± 0.01 (0.674)	0.05 ± 0.01 (0.915)
Femur length (mm)	13.9 ± 0.1 (0.967)	14.0 ± 0.1	14.1 ± 0.1 (0.980)	14.0 ± 0.1 (0.999)	14.2 ± 0.1 (0.898)
Marrow adipose tissue (%)	0.6 ± 0.2 (0.498)	1.0 ± 0.4	0.4 ± 0.1 (0.123)	0.2 ± 0.1 (0.043)	1.2 ± 0.2 (0.960)
Non fasting glucose (mmol/l)	9.7 ± 0.4 (0.574))	10.5 ± 0.6	10.6 ± 0.6 (>0.999)	10.7 ± 0.3 (0.627)	10.6 ± 0.3 (>0.999)
CTx-I (ng/ml)	8.9 ± 0.5 (<0.001)	14.7 ± 1.0	9.2 ± 0.7 (<0.001)	9.4 ± 1.0 (0.02)	10.8 ± 1.0 (<0.001)
P1NP (ng/ml)	20.4 ± 1.7 (0.062)	26.4 ± 1.3	23.6 ± 1.9 (0.680)	21.3 ± 2.1 (0.120)	22.5 ± 1.3 (0.340)

Data are presented as mean ± SEM (p value). Data have been analyzed by one-way ANOVA followed by *post hoc* Dunnett's multiple comparison test using OVX+Veh group as the control group. Bold values represent significant differences as compared with OVX+Veh. CTx-I: C-terminal telopeptide of type I collagen, P1NP: N-terminal propeptide of type I procollagen.

**Table 3. Cortical bone microarchitectural parameters at the midshaft tibia.**

	Sham+Veh	OVX+Veh	OVX+GIP <sub>1-30</sub>	OVX+GIP-Tag	OVX+Aln
Tt.Ar (mm <sup>2</sup> )	1.72 ± 0.04 (0.025)	1.54 ± 0.04	1.70 ± 0.03 (0.042)	1.66 ± 0.03 (0.221)	1.51 ± 0.08 (0.988)
Ma.Ar (mm <sup>2</sup> )	0.71 ± 0.02 (0.005)	0.61 ± 0.02	0.71 ± 0.01 (0.004)	0.67 ± 0.01 (0.208)	0.63 ± 0.03 (0.873)
Ct.Ar (mm <sup>2</sup> )	1.00 ± 0.02 (0.038)	0.90 ± 0.01	0.98 ± 0.02 (0.044)	0.96 ± 0.03 (0.378)	0.87 ± 0.05 (0.747)
Ct.Th (μm)	245 ± 3 (0.411)	236 ± 5	230 ± 5 (0.630)	235 ± 4 (0.997)	225 ± 6 (0.740)
Iap (mm <sup>4</sup> )	0.23 ± 0.01 (0.814)	0.22 ± 0.02	0.24 ± 0.01 (0.538)	0.22 ± 0.01 (0.990)	0.24 ± 0.03 (0.815)
Iml (mm <sup>4</sup> )	0.26 ± 0.00 (0.648)	0.24 ± 0.01	0.27 ± 0.01 (0.297)	0.28 ± 0.01 (0.081)	0.19 ± 0.02 (0.028)
J (mm <sup>4</sup> )	0.49 ± 0.03 (0.347)	0.44 ± 0.02	0.52 ± 0.01 (0.049)	0.48 ± 0.02 (0.648)	0.41 ± 0.04 (0.800)

Data are presented as mean ± SEM (p value). Data have been body-size adjusted with a linear regression method and analyzed by one-way ANOVA followed by *post hoc* Dunnett's multiple comparison test using OVX+Veh group as the control group. Bold values represent significant differences as compared with OVX+Veh. Tt.Ar: total cross-sectional area, Ma.Ar: medullary area, Ct.Ar: cortical bone area, Ct.Th: cortical thickness, Iap: moment of inertia about the anteroposterior axis, Iml: moment of inertia about the mediolateral axis, J: polar moment of inertia

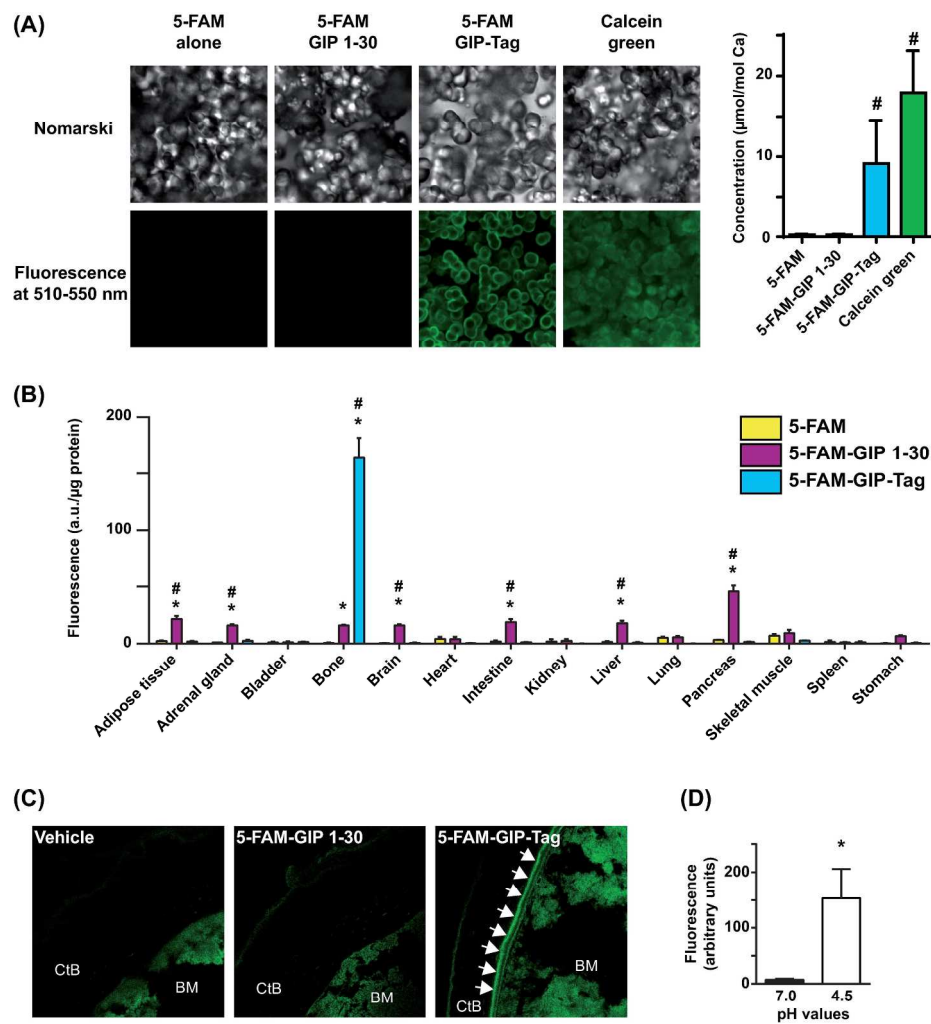


Figure 1

219x285mm (300 x 300 DPI)



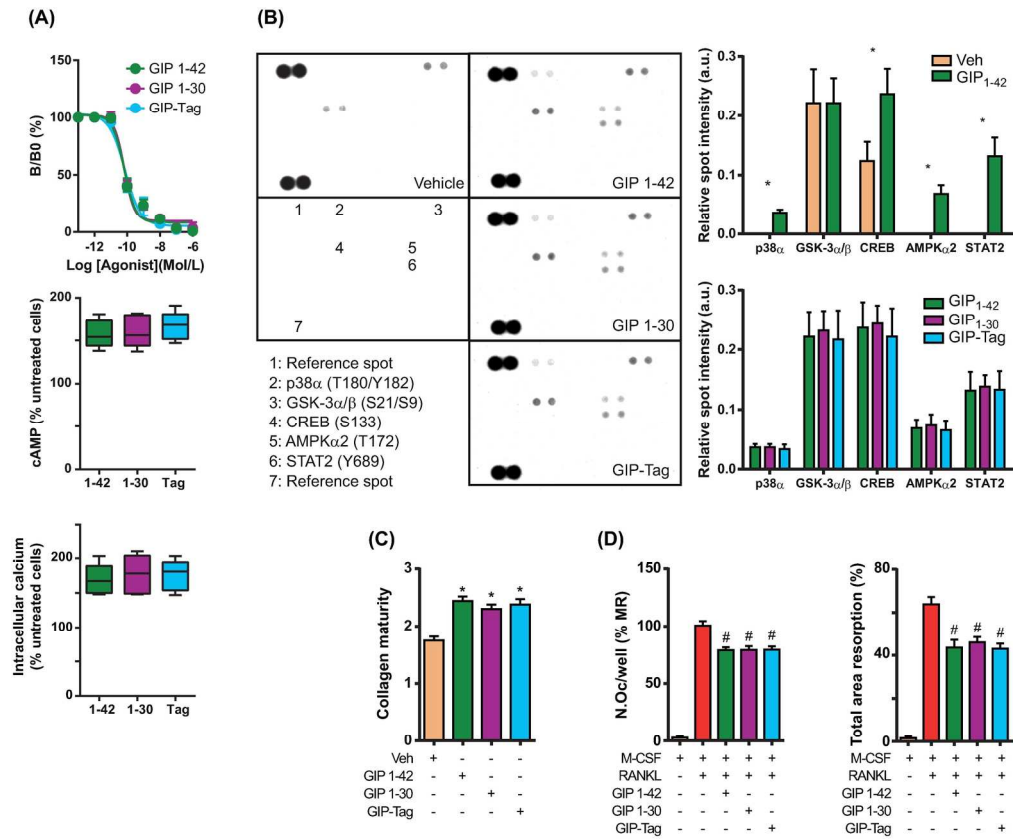


Figure 2

185x192mm (300 x 300 DPI)

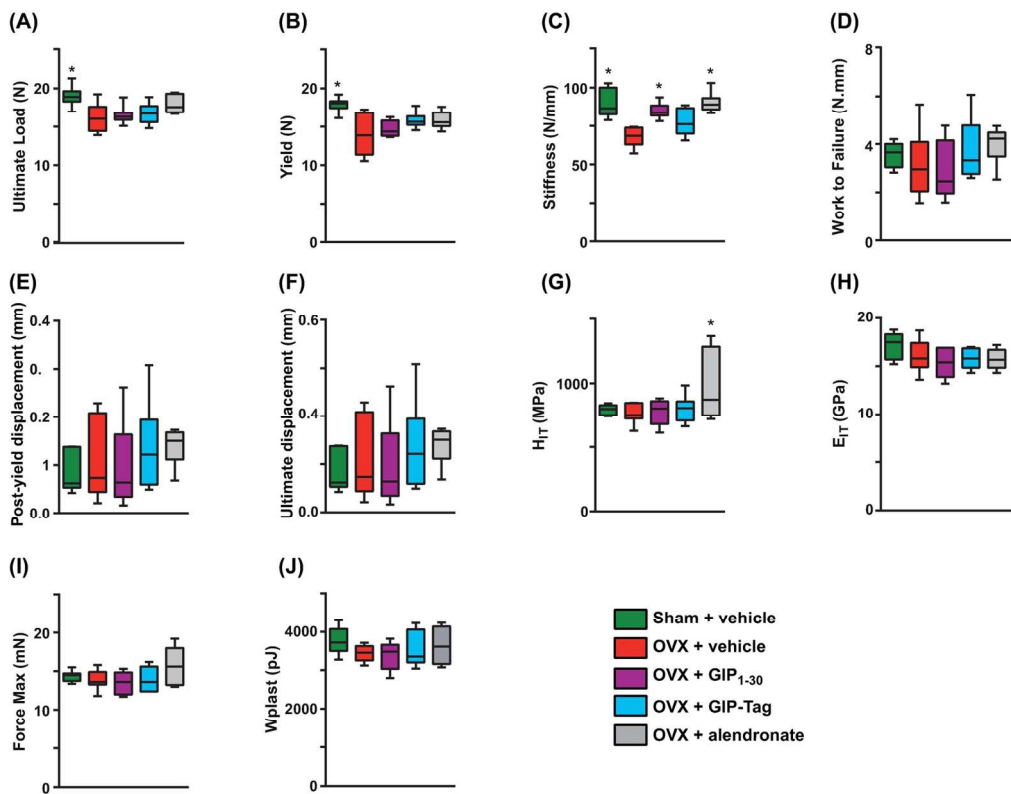


Figure 3

150x137mm (300 x 300 DPI)

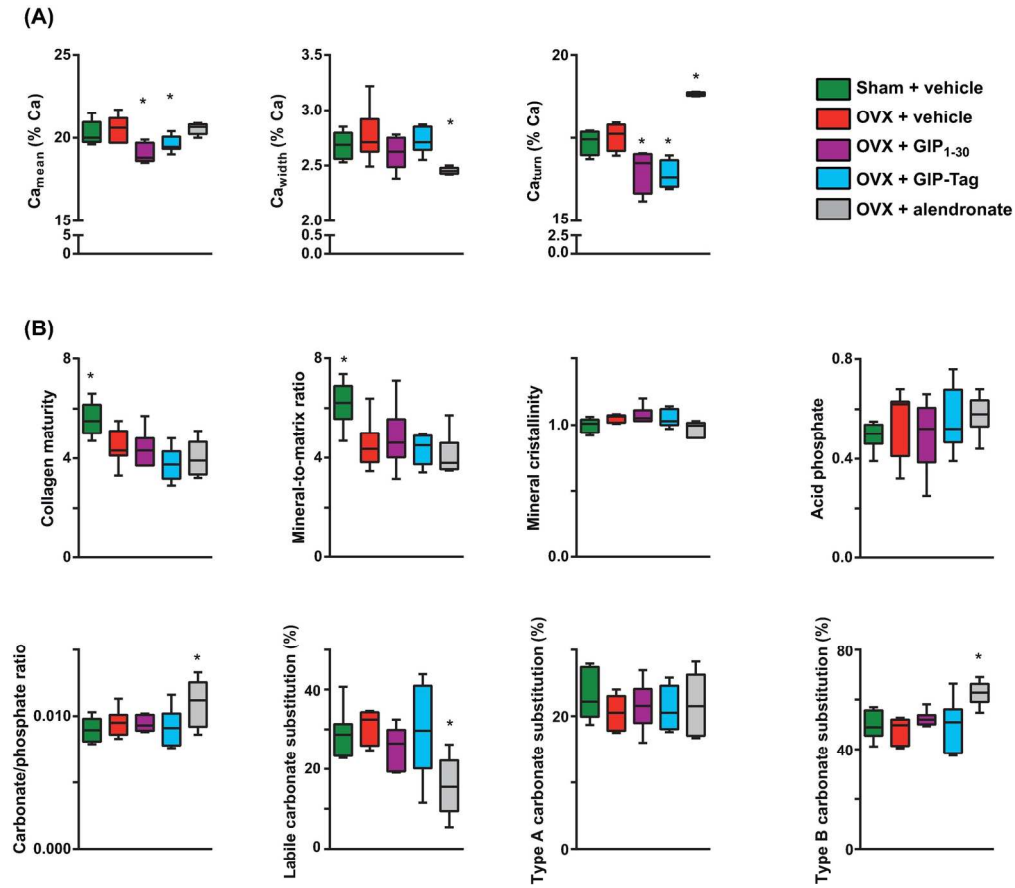


Figure 4

171x183mm (300 x 300 DPI)